Out-of-plane (e,2e) measurements and calculations on He autoionizing levels as a function of incident-electron energy

N. L. S. Martin, C. M. Weaver, B. N. Kim, B. A. deHarak, O. Zatsarinny, and K. Bartschat

Phys. Rev. A **97**, 052710 — Published 29 May 2018

DOI: 10.1103/PhysRevA.97.052710

Out-of-plane $(e, 2e)$ measurements and calculations on He autoionizing levels as a function of incident-electron energy.

N. L. S. Martin,[1] C. M. Weaver,[1] B. N. Kim,[1]

B. A. deHarak,[2] O. Zatsarinny,[3] and K. Bartschat[3]

[1]*Department of Physics and Astronomy,*

University of Kentucky, Lexington, Kentucky 40506-0055, USA

[2]*Physics Department, Illinois Wesleyan University,*

P.O. Box 2900, Bloomington, IL 61702-2900, USA

[3]*Department of Physics and Astronomy,*

Drake University, Des Moines, IA 50311, USA

Abstract

Out-of-scattering-plane $(e, 2e)$ measurements and calculations are reported for the three singlet helium $2\ell 2\ell'$ autoionizing levels, with 80, 100, 120, 150, and 488 eV incident-electron energies, and scattering angles 60°, 50.8°, 45°, 39.2°, and 20.5°, respectively. The kinematics are the same in all cases: the momentum transfer is $K = 2.1$ a.u., and ejected electrons are detected in a plane that contains the momentum transfer direction and is perpendicular to the scattering plane. The results are presented as $(e, 2e)$ angular distributions energy-integrated over each level. They are compared with fully nonperturbative B-spline R-matrix and hybrid second-order distorted-wave + R-matrix calculations.

PACS numbers: 34.80.Dp

I. INTRODUCTION

The electron-impact ionization of helium, via the singlet $2\ell 2\ell'$ autoionizing levels, $(2s^2)^1S$, $(2p^2)^1D$, and $(2s2p)^1P$, has been extensively studied [1–13] using the electron-electron coincidence or $(e,2e)$ technique [14, 15]. For such $(e,2e)$ experiments an electron e_0 is incident on a He atom, and the ejected electron e_{ej} is observed in coincidence with the scattered electron e_{sc} for the overall process

$$\begin{array}{ccc} \mathrm{He}(1s^2) + e_0 & \longrightarrow & \mathrm{He}^+(1s) + e_{sc} + e_{ej}. \\ & \searrow \mathrm{He}\ (2\ell 2\ell') \nearrow & \end{array} \tag{1}$$

Even though the two outgoing electrons are, in principle, indistinguishable, we use the common notation of referring to the faster one as "scattered" and the slower one as "ejected".

We are particularly interested in cases, where there is interference between the amplitudes for direct ionization (upper path) and autoionization via an intermediate resonance (lower path) [16]. The ejected-electron energies for the three autoionizing levels are $E_{ej}(^1S) = 33.25$ eV, $E_{ej}(^1D) = 35.32$ eV, $E_{ej}(^1P) = 35.56$ eV [17, 18], and the corresponding scattered-electron energies are $E_{sc} = E_0 - E_I - E_{ej}$, where E_0 is the incident-electron energy and $E_I = 24.59$ eV is the first ionization potential of He.

Three geometries, shown in Fig. 1, have been used for $(e,2e)$ experiments on He. Figure 1(a) highlights the coplanar geometry (plane I), where the ejected-electron momentum $\boldsymbol{k}_{ej}$ lies in the scattering plane formed by the incident-electron momentum $\boldsymbol{k}_0$ and the scattered-electron momentum $\boldsymbol{k_{sc}}$; the momentum transfer, $\boldsymbol{K} = \boldsymbol{k}_0 - \boldsymbol{k}_{sc}$, also lies in this plane. Coplanar experiments measure the $(e,2e)$ ejected electron angular distribution as a function of χ, the angle between $\boldsymbol{k}_0$ and $\boldsymbol{k}_{ej}$.

Figure 1(b) highlights the true "perpendicular plane" geometry (plane II), where the ejected electron lies in a plane that is perpendicular to both the scattering plane and the momentum-transfer direction. Here the $(e,2e)$ ejected electron angular distribution is a function of the polar angle θ_{ej} shown in the figure. $(e,2e)$ experiments on *direct* ionization have yielded data for this plane as a slice through 3D COLTRIMS ejected-electron angular distributions [19]; *i.e.,* for ejected-electron energies away from the autoionizing region and hence corresponding only to the upper path of Eq. (1).

Figure 1(c) highlights a special out-of-plane "perpendicular plane" geometry (plane III),

where the ejected electron lies in a plane that is perpendicular to the scattering plane but contains the momentum-transfer direction. The (e,2e) ejected electron angular distribution is a function of the azimuthal angle ϕ shown in the figure. Our experiments are performed with this geometry, which was readily available by modifying an existing coplanar (e,2e) apparatus [20].

Our original out-of-plane experiments were stimulated by ion-atom ionization studies of C^{6+} on He [21], and (e,2e) experiments on He [19]. Both these experiments used the COLTRIMS technique to obtain full 3D ejected-electron angular distributions. It was found that, contrary to expectations for the kinematics employed, the results of these experiments disagreed with predictions from first-order theoretical calculations. It also turned out that our experiments were of interest in their own right: the geometry of Fig. 1(c) enabled the observation of both the binary and recoil peaks (along $\hat{\boldsymbol{K}}$ and $-\hat{\boldsymbol{K}}$, respectively) as well as part of the out-of-plane region. All our out-of-plane experiments reported to date have been carried out at the relatively high incident energy of 488 eV. Three types of experiment have been carried out: (i) (e,2e) ejected-electron angular distribution measurements that energy-integrated over each autoionizing level [22], (ii) (e,2e) ejected-electron angular distribution measurements that obtained energy spectra over each autoionizing level [23], and (iii) the (e,2e) recoil-peak to binary-peak ratio as a function of ejected-electron energy across the He$(2p^2)^1D$ and $(2s2p)^1P$ levels [24].

It was found that all three types of high-energy experiments were in good agreement with predictions from a hybrid second-order distorted-wave + R-matrix (close-coupling) calculation (see next section), but were not in good agreement with an equivalent first-order calculation. This is traceable to the fact that the electron-impact ionization of He, via the doubly-excited autoionizing levels, is a true four-body process, even at high incident energy; a calculation, therefore, requires a second-order term that describes the interaction of the projectile with both atomic electrons [25].

We have now carried out a comprehensive series of type (i) out-of-plane (e,2e) experiments at lower incident-electron energies. All our experiments are for the special kinematical case where the momentum transfer vector is perpendicular to the scattered electron direction (see Fig 1(c)). For an incident electron with energy E_0, the condition for this is a scattering angle $\theta_{sc} = \arcsin\left(\sqrt{\Delta E/E_0}\right)$, where $\Delta E = E_I + E_{ej}$ is the energy loss, *i.e.,* the energy of the $2\ell 2\ell'$ autoionizing levels above the ground state ≈ 60 eV. The momentum transfer

is then given by $K = \sqrt{2\Delta E}$, which is independent of the initial energy and has the value $K = 2.1$ a.u. in the autoionizing region. The experiments reported below were carried out for incident energies $E_0 = 150, 120, 100,$ and 80 eV. Table I gives the corresponding scattering angles for these energies, and also for our original 488 eV experiment.

Section II gives some details of the theoretical models with whose predictions we compare the experimental results. Section III describes the apparatus and the geometry of our out-of-plane measurements. Section IV presents the results, and Section V our summary and conclusions.

II. THEORY

Our 488 eV experiments were compared with high-energy state of the art first-order and second-order hybrid distorted-wave + convergent R-matrix with pseudo-states (close-coupling) calculations (DWB1-RMPS and DWB2-RMPS, respectively). The DWB1-RMPS and DWB2-RMPS methods are described in detail elsewhere [26–29]: the (fast) projectile−target interaction is treated perturbatively to first (DWB1) or second (DWB2) order, while the initial bound state and the e−He^+ half-collision of a slow ejected electron and the residual ion are treated via a convergent close-coupling expansion. As stated above, the second-order, but not the first-order, calculations were in good agreement with the experiments.

For comparison with the present experiments, calculations suitable for lower incident electron energies have been carried out using the B-spline R-matrix with pseudostates method (BSRMPS) [30]. The essential point is a two-step model: We first calculate amplitudes for *excitation* of the pseudostates, and then we use a projection scheme with weighting factors determined by the overlap of the pseudostates with the true e–He^+ scattering state for the ejected electron. Although this projection recipe does not have a formal origin [31], due to the fact that the individual pseudostates and the continuum state of interest have *different* energies, the above scheme has been very successful. In fact, it is applicable to general targets, as well as to cases such as simultaneous ionization plus excitation [32–34].

Figure 2 shows the results of these calculations at 150, 120, 100, and 80 eV incident energies, for direct ionization (*i.e.,* for an ejected-electron energy away from the autoionizing region) and for ejected-electron energies corresponding to the three autoionizing levels; all

angular distributions are normalized to unity in the binary peak. Also included in the figure are the original calculations for 488 eV [22]. All calculations have been integrated over a uniform energy window of 0.4 eV corresponding to the experimental setup. For direct ionization and the ^1S autoionizing level, there is essentially no recoil peak at any energy. For the ^1D and ^1P autoionizing levels, there is a recoil peak that decreases (relative to the binary peak) as the incident-electron energy decreases, finally vanishing at 80 eV. The binary peak width varies with energy in a nontrivial manner. For direct ionization and the ^1S level, the binary peak width is the same for all energies except 80 eV, for which it is narrower. For the ^1D and ^1P autoionizing levels it is the same for the three highest energies; the two lowest energies are the same as each other and narrower. Lastly, the out-of-plane region between 30° and 120° does not appear to exhibit a simple trend as the incident-electron energy decreases.

Overall, there is a strong similarity between the results for the various incident projectile energies ≥ 100 eV. Since the calculations at all energies have the same value of momentum transfer ($K = 2.1$ au) it is tempting to assume that this is the overriding reason why the shape of the angular distributions are similar. In particular, there is the possibility that the DWB2-RMPS may give the same results at much lower incident energies than 488 eV. Such an assumption is valid for the *first* Born approximation where matrix elements depend only on K and not on k_0 and k_{sc} separately, but it is not expected to be valid for a *second* Born calculation which involves sums over the products of intermediate-state matrix elements, with values of intermediate momentum transfers that vary with incident-electron energy, and scattering angle. To investigate this we have carried out DWB2-RMPS calculations for 150 eV incident energy. The results are shown in Fig. 3, where they are compared with the original 488 eV DWB2-RMPS results and the new 150 eV BSRMPS calculations; all calculations are normalized in the binary peak. As can be seen, the 150 eV DWB2-RMPS results do not agree with the 488 eV in both the out-of-plane and the recoil peak regions: there are similar features, but they are greatly enhanced at 150 eV, with recoil peaks up to a factor of three larger. Thus the common value of the momentum transfer cannot be the cause of the similarities between the results of the 488 eV DWB2-RMPS and 150 eV BSRMPS calculations. A thorough investigation of this phenomenon is outside the scope of this paper.

We do not expect any similarity with the high incident-energy results for the 80 eV

BSRMPS calculations. In this case, the energy loss is so large that the "scattered" projectile has less energy that the "ejected" electron, i.e., their roles are switched and the simplified labeling of the two outgoing electrons is no longer valid. In other words, exchange effects between the projectile and the target electrons should be very important. These effects are included in BSRMPS, but not in the DWB2-RMPS model.

III. EXPERIMENT

The experimental apparatus is described in detail elsewhere [20, 35]. It consists of an unmonochromated electron gun, a gaseous target beam, two ejected-electron spectrometers, and a scattered-electron spectrometer. The two ejected-electron spectrometers are at angles $\pm 90^\circ$ with respect to the scattered-electron spectrometer. The gun can move on the surface of a cone of half-angle θ_{sc} whose axis lies in the scattered-electron detector direction. This is illustrated in Fig. 4, which shows the trajectories of the incident, scattered, and ejected electrons. This geometry is equivalent to rotating the ejected electron detectors around $\boldsymbol{z}$ while keeping the gun and scattered electron detector fixed. Thus, as the gun position is varied from $\phi = 0 \rightarrow 180^\circ$, the ejected detector on the left effectively varies from $\phi_{ej} = 0 \rightarrow -180^\circ$, and the ejected detector on the right effectively varies from $\phi_{ej} = 180 \rightarrow 0^\circ$, with a combined range equal to the full $\phi_{ej} = 0 \rightarrow 360^\circ$. Kinematically this yields angular-distribution measurements corresponding to Fig. 1(c). The binary peak position (*i.e.,* momentum transfer direction) corresponds to $\phi = 0$ and the recoil peak position to $\phi = 180^\circ$.

For measurements at each incident-electron energy the scattering angle θ_{sc} was fixed at the value given by Table I. This required the positioning of the gun to the appropriate θ_{sc} on the mounting arm shown in Fig. 2 of Ref. [20]. Careful alignment was necessary to ensure that the electron beam accurately intersected the interaction region for all values of ϕ. For the low energy experiments reported below, a new electron gun was used which gave a tightly focused and well collimated electron beam; it was found that the data did not then need to be corrected for an instrument function, as was done for the 488 eV data [20].

For the angular distribution measurements, the apparatus was tuned to accept electrons in a uniform energy window of 0.4 eV [35]. As stated above, the theoretical predictions were energy-integrated over the same window.

IV. RESULTS AND DISCUSSION

The experimental results and theoretical predictions are shown in Fig. 5. The 488 eV experimental results and theoretical calculations are those from Ref. [22], except that only the second-order calculations are shown. All calculations have been normalized to the experimental data in the binary peak.

In general the agreement between theory and experiment is quite good. For all incident-electron energies down to 100 eV the angular distributions have a pronounced recoil peak for both the $(2p^2)^1D$ and $(2s2p)^1P$. For 150 eV, 120 eV, and 100 eV, the angular distributions are quite similar to one another and to the 488 eV data, although the experimental statistical uncertainties of the lower energy data are too large to probe the fine details of the predicted angular distributions.

In view of these similarities, the 150 eV, 120 eV, and 100 eV experimental angular distributions may be summed to improve the statistics. The result is shown in Fig. 6, where the summation of each data point is weighted by its statistical uncertainty in the usual manner; as can be seen, the quality of the angular distributions is much improved. Also shown in the figure are the calculations for incident energies 488 eV and 120 eV – the latter is approximately the mean energy of the summed distributions. For direct ionization the two calculations are indistinguishable from each other except in the out-of-plane region between 30° and 90°; in this region neither calculation describes the data perfectly. This is also true of the $(2s^2)^1S$ autoionizing level, although the low-energy BSRMPS calculation is slightly better overall. The situation is quite different for the $(2p^2)^1D$ and $(2s2p)^1P$ levels for which there is a pronounced recoil peak. For $(2p^2)^1D$, both the recoil peak and the out-of-plane region are much better described by the 488 eV DWB2-RMPS calculation. For $(2s2p)^1P$, the recoil peak is almost perfectly described by this model, whereas in the out-of-plane region neither calculation is satisfactory; both predict a small subsidiary peak which is either absent, or extremely small, in the experimental data.

We now turn to the lowest-energy angular distributions for 80 eV shown in the right panels of Fig. 5. As predicted by the BSRMPS calculations, the angular distributions are very different from those at the higher energies. The binary peak is much narrower, with a half width of about 15°, and the recoil peak for the $(2p^2)^1D$ and $(2s2p)^1P$ levels has vanished. The experiments at this energy were run for much longer than at the other energies in order

to obtain statistics good enough to confirm the dramatic differences between this energy and the higher energies.

V. SUMMARY AND CONCLUSIONS

We have carried out a comprehensive set of experiments that examine out-of-plane $(e,2e)$ ejected-electron angular distributions of He autoionizing states, for a range of incident-electron energies that varies by a factor of six. The results are in quite good, but not perfect, agreement with state-of-the-art low incident-electron energy calculations. It is found that the angular distributions – in particular the binary and recoil peaks – do not vary noticeably for electron energies 100 eV – 488 eV, and are in fact well described by the high-energy calculations. On the other hand, at the lowest incident energy of 80 eV, there is no recoil peak for any of the autoionizing levels, and the binary peak is narrower than at higher energies. The 80 eV data are almost perfectly described by the low-energy BSRMPS calculations.

For the $2\ell 2\ell'$ autoionizing region the energy loss is about 60 eV. Thus, it appears to be significant that, for $E_0 \geq 100$ eV, the scattered-electron energy is greater than the ejected-electron energy of $\sim$35 eV. For 80 eV, however, the roles are interchanged, and hence electron-exchange effects are very important.

Acknowledgments

This work was supported by the United States National Science Foundation under Grants No. PHY-0855040 and PHY-1607140 (NLSM), PHY-1402899 and PHY-1708108 (BAd), PHY-1403245 (KB), and PHY-1520970 (OZ & KB).

[1] E. Weigold, A. Ugbabe, and P. J. O. Teubner, Phys. Rev. Lett. **35**, 209 (1975), URL `https://link.aps.org/doi/10.1103/PhysRevLett.35.209`.

[2] J. Lower and E. Weigold, Journal of Physics B: Atomic, Molecular and Optical Physics **23**, 2819 (1990), URL `http://stacks.iop.org/0953-4075/23/i=16/a=023`.

[3] O. Samardzic, J.-A. Hurn, E. Weigold, and M. J. Brunger, Aust. J. Phys **47**, 703 (1994).

[4] O. Samardzic, A. S. Kheifets, E. Weigold, B. Shang, and M. J. Brunger, Journal of Physics B: Atomic, Molecular and Optical Physics **28**, 725 (1995), URL http://stacks.iop.org/0953-4075/28/i=4/a=020.

[5] M. J. Brunger, O. Samardzic, A. S. Kheifets, and E. Weigold, Journal of Physics B: Atomic, Molecular and Optical Physics **30**, 3267 (1997), URL http://stacks.iop.org/0953-4075/30/i=14/a=017.

[6] O. Samardzic, L. Campbell, M. J. Brunger, A. S. Kheifets, and E. Weigold, Journal of Physics B: Atomic, Molecular and Optical Physics **30**, 4383 (1997), URL http://stacks.iop.org/0953-4075/30/i=19/a=024.

[7] A. Pochat, R. J. Tweed, M. Doritch, and J. Peresse, Journal of Physics B: Atomic and Molecular Physics **15**, 2269 (1982), URL http://stacks.iop.org/0022-3700/15/i=14/a=017.

[8] M. J. Coggiola, D. L. Huestis, and R. R. Saxon, eds., *Proceedings of the 14th International Conference on Physics of Electronic and Atomic Collisions* (Stanford University Press, 1985).

[9] G. Stefani, ed., *Proceedings of the 2nd European Conference on (e,2e) Collisions and Related Problems* (Montelibretti, 1990).

[10] D. G. McDonald and A. Crowe, Zeitschrift für Physik D Atoms, Molecules and Clusters **23**, 371 (1992), ISSN 1431-5866, URL https://doi.org/10.1007/BF01429260.

[11] D. G. McDonald and A. Crowe, Journal of Physics B: Atomic, Molecular and Optical Physics **26**, 2887 (1993), URL http://stacks.iop.org/0953-4075/26/i=17/a=021.

[12] O. Sise, M. Dogan, I. Okur, and A. Crowe, Journal of Physics B: Atomic, Molecular and Optical Physics **43**, 185201 (2010), URL http://stacks.iop.org/0953-4075/43/i=18/a=185201.

[13] O. Sise, M. Dogan, I. Okur, and A. Crowe, Phys. Rev. A **84**, 022705 (2011), URL https://link.aps.org/doi/10.1103/PhysRevA.84.022705.

[14] H. Ehrhardt, M. Schulz, T. Tekaat, and K. Willmann, Phys. Rev. Lett. **22**, 89 (1969), URL https://link.aps.org/doi/10.1103/PhysRevLett.22.89.

[15] U. A. Jr., A. Egidi, R. Marconero, and G. Pizzella, Review of Scientific Instruments **40**, 1001 (1969), http://dx.doi.org/10.1063/1.1684135, URL http://dx.doi.org/10.1063/1.1684135.

[16] U. Fano, Phys. Rev. **124**, 1866 (1961).

[17] J. P. van den Brink, G. Nienhuis, J. van Eck, and H. G. M. Heideman, J. Phys. B **22**, 3501 (1989).

[18] B. A. deHarak, J. G. Childers, and N. L. S. Martin, Phys. Rev. A **74**, 032714 (2006).

[19] M. Dürr, C. Dimopoulou, B. Najjari, A. Dorn, and J. Ullrich, Phys. Rev. Lett. **96**, 243202 (2006).

[20] B. A. deHarak and N. L. S. Martin, Meas. Sci. Technol. **19**, 015604 (2008).

[21] M. Schulz, R. Moshammer, D. Fischer, H. Kollmus, D. H. Madison, S. Jones, and J. Ullrich, Nature **422**, 48 (2003).

[22] B. A. deHarak, K. Bartschat, and N. L. S. Martin, Phys. Rev. Lett. **100**, 063201 (2008).

[23] B. A. deHarak, K. Bartschat, and N. L. S. Martin, Phys. Rev. A **82**, 062705 (2010), URL `http://link.aps.org/doi/10.1103/PhysRevA.82.062705`.

[24] B. A. deHarak, K. Bartschat, and N. L. S. Martin, Phys. Rev. A **89**, 012702 (2014), URL `http://link.aps.org/doi/10.1103/PhysRevA.89.012702`.

[25] N. L. S. Martin, B. A. deHarak, and K. Bartschat, J. Phys. B **42**, 225201 (2009).

[26] K. Bartschat and P. G. Burke, J. Phys. B **20**, 3191 (1987).

[27] R. H. G. Reid, K. Bartschat, and A. Raeker, J. Phys. B **31**, 563 (1998), *corrigendum:* J. Phys. B **33**, 5261 (2000).

[28] Y. Fang and K. Bartschat, J. Phys. B **34**, L19 (2001).

[29] K. Bartschat and A. N. Grum-Grzhimailo, J. Phys. B **35**, 5035 (2002).

[30] O. Zatsarinny and K. Bartschat, Physical Review A **85**, 062709 (2012).

[31] I. Bray, C. J. Guilfoile, A. S. Kadyrov, D. V. Fursa, and A. T. Stelbovics, Physical Review A **90**, 022710 (2014).

[32] O. Zatsarinny and K. Bartschat, Physical Review Letters **107**, 023203 (2011).

[33] O. Zatsarinny and K. Bartschat, J. Phys. B **46**, 112001 (2013).

[34] O. Zatsarinny and K. Bartschat, Physical Review A **93**, 012712 (2016).

[35] B. A. deHarak, J. G. Childers, and N. L. S. Martin, J. Elec. Spec. Rel. Phen. **141**, 75 (2004).

TABLE I: Incident electron energies and the corresponding scattering angles, in the He $2\ell 2\ell'$ autoionizing region, for the condition that the momentum transfer vector is perpendicular to the scattered electron direction. The momentum transfer is 2.1 a.u. in all cases.

E_0(eV)	θ_{sc}°
488	20.5
150	39.2
120	45
100	50.8
80	60

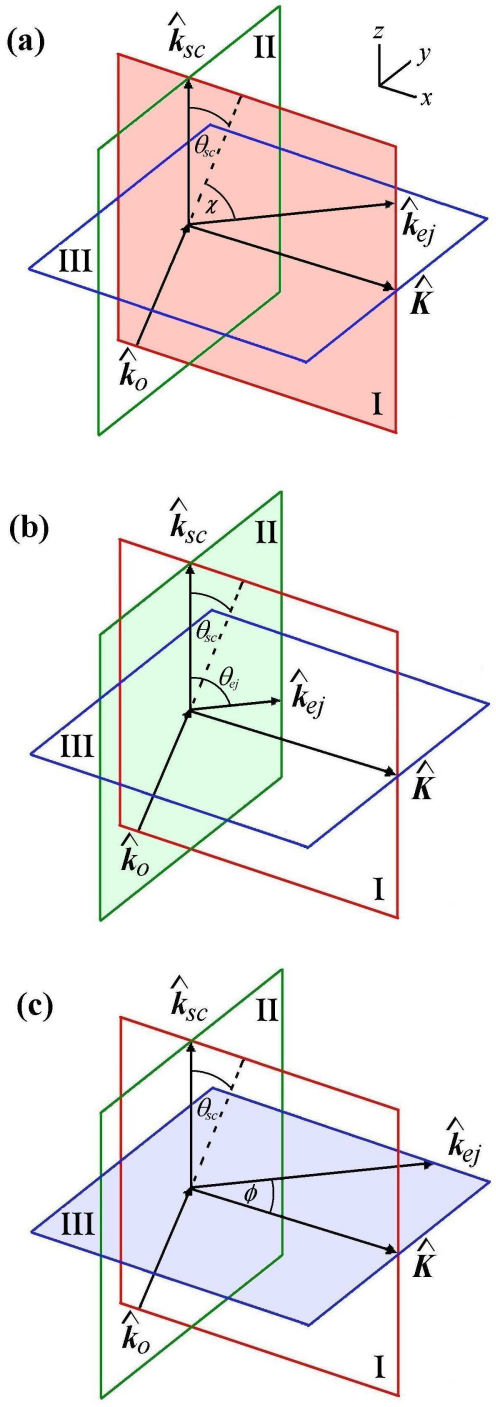

FIG. 1: Three types of $(e,2e)$ experimental geometry in which the ejected electron is detected in (a) the scattering plane I that contains the incident electron, the scattered electron, and the momentum transfer, directions, (b) the *perpendicular plane* II that is normal to the momentum transfer direction, (c) plane III that is perpendicular to the scattering plane but contains the momentum transfer direction; this is the out-of-plane geometry used in the present experiments.

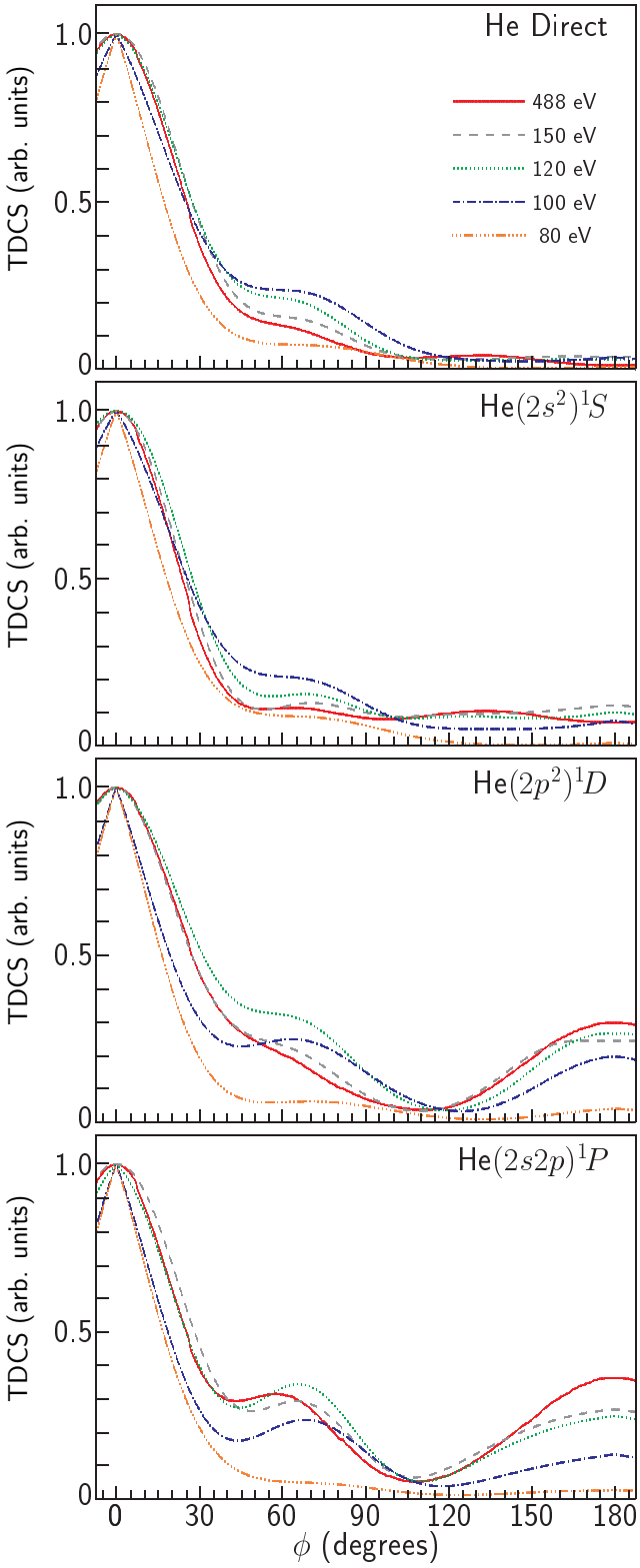

FIG. 2: Calculated (e,2e) ejected-electron angular distributions described in the text. The incident-electron energies correspond to the experiments described below. The 488 eV is a DWB2-RMPS calculation, and the remainder are BSRMPS calculations.

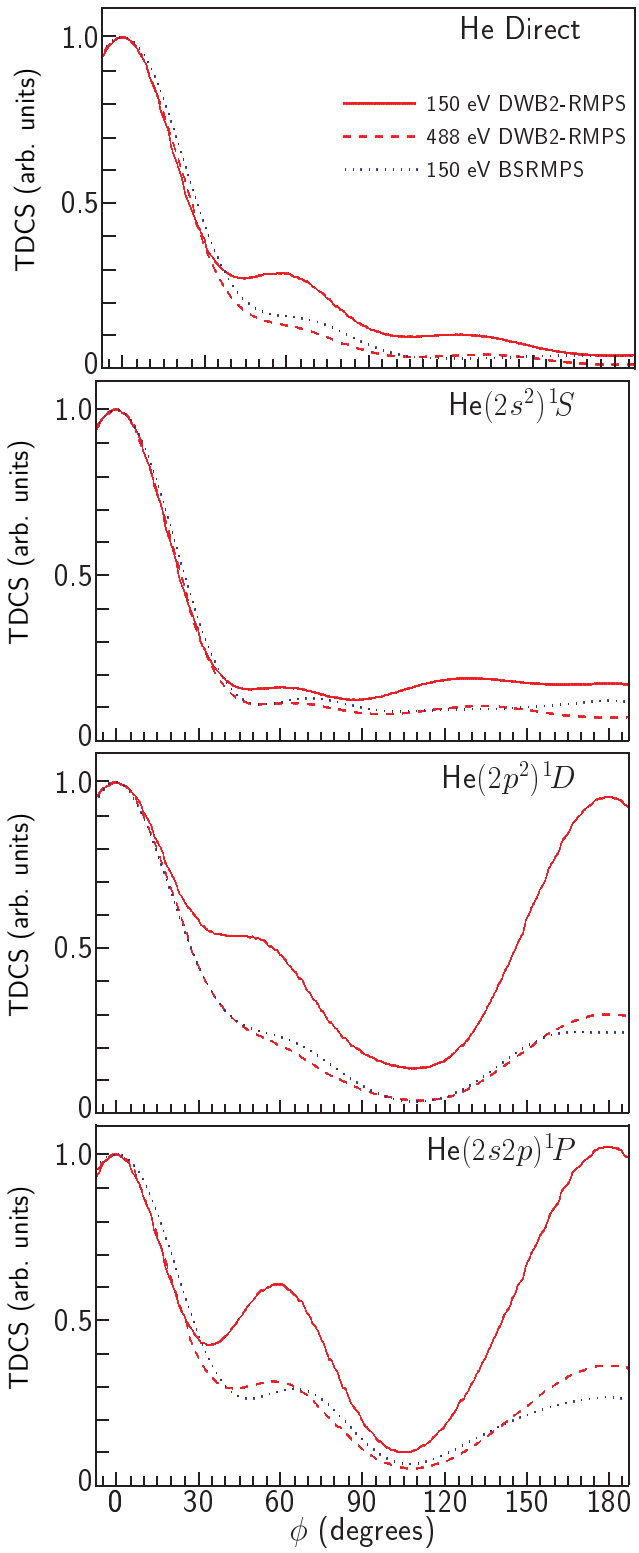

FIG. 3: DWB2-RMPS calculations of the $(e,2e)$ ejected-electron angular distributions for 150 eV and 488 eV incident energy compared with the 150 eV BSRMPS calculations. All calculations are normalized in the binary peak. See text for details.

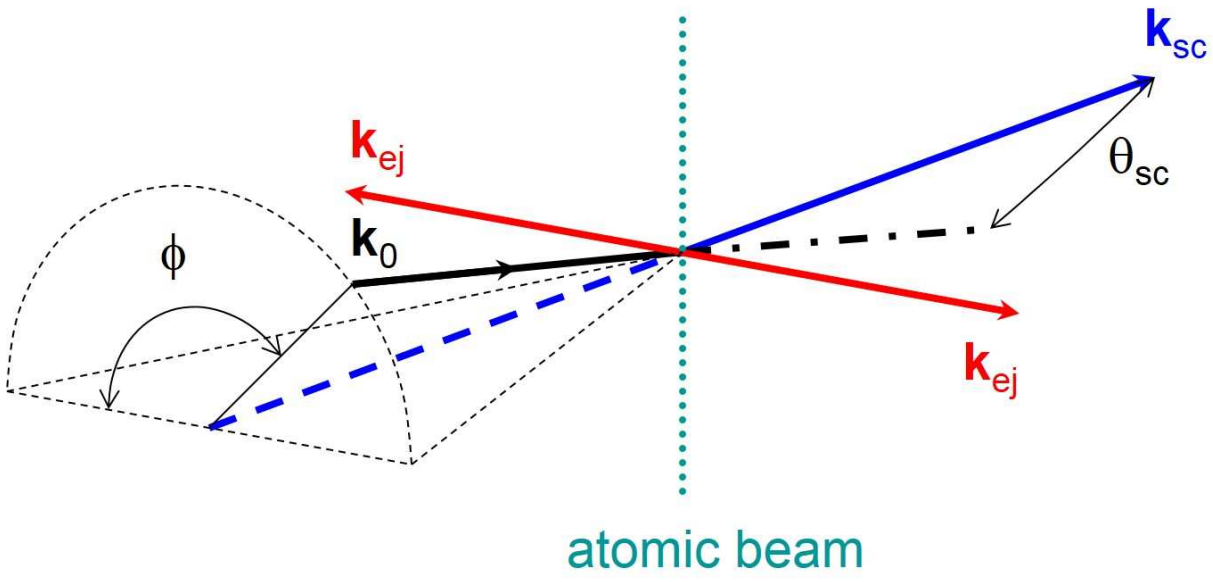

FIG. 4: Geometry of the apparatus. The incident ($\boldsymbol{k}_0$) and detected ejected ($\boldsymbol{k}_{ej}$) and scattered ($\boldsymbol{k}_{sc}$) electron directions are indicated.

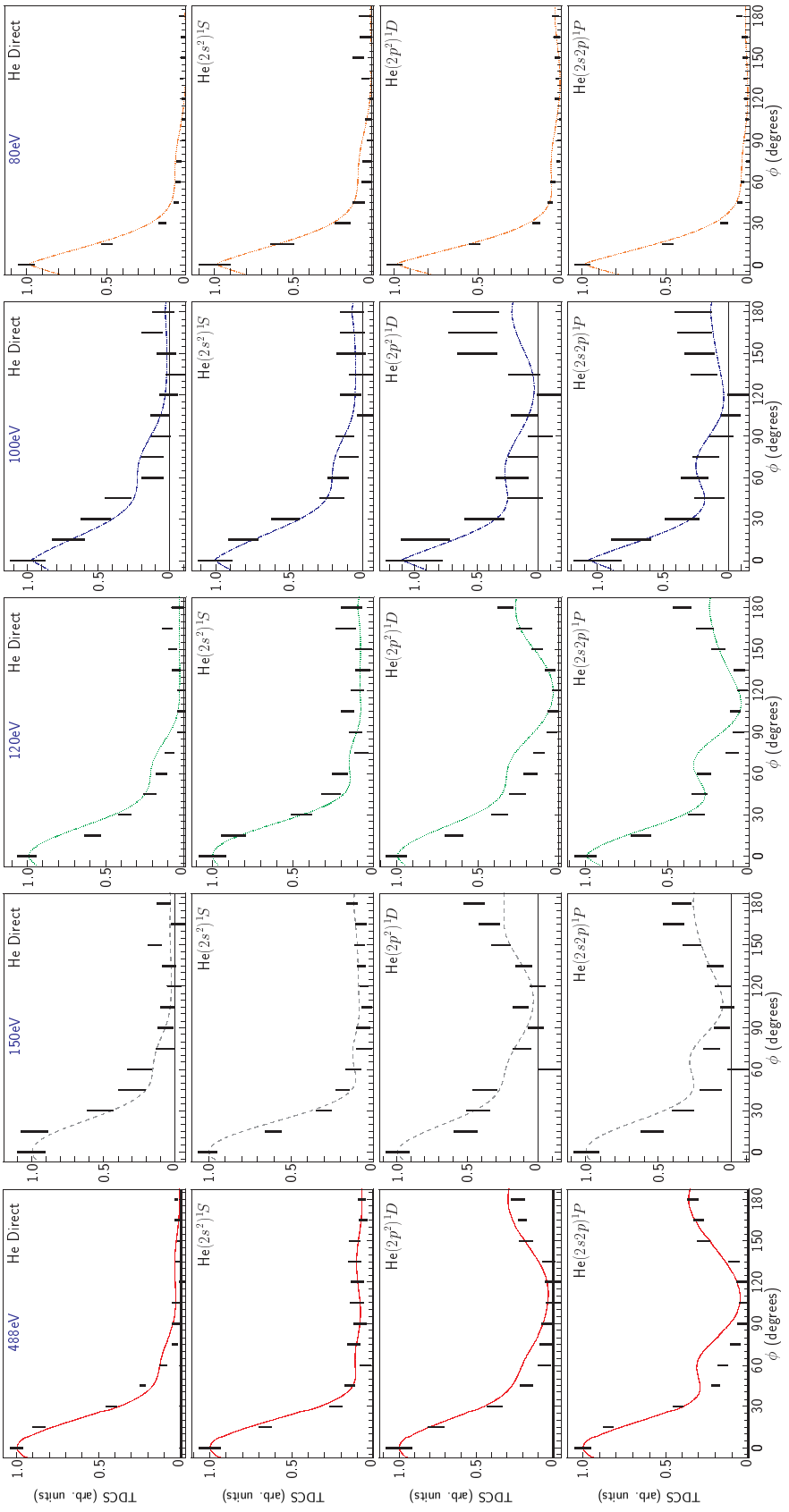

FIG. 5: Out-of-plane $(e,2e)$ angular distributions, for helium direct ionization and the $(2s^2)^1S$ $(2p^2)^1D$ and $(2s2p)^1P$ autoionizing resonances, for 488, 150, 120, 100, and 80 eV incident electron energy. The corresponding scattering angles are given in Table I. The vertical bars represent the experimental results and indicate the statistical errors. The theoretical curves are those from Fig. 2. Theory and experiment are normalized to unity at $\phi = 0$.

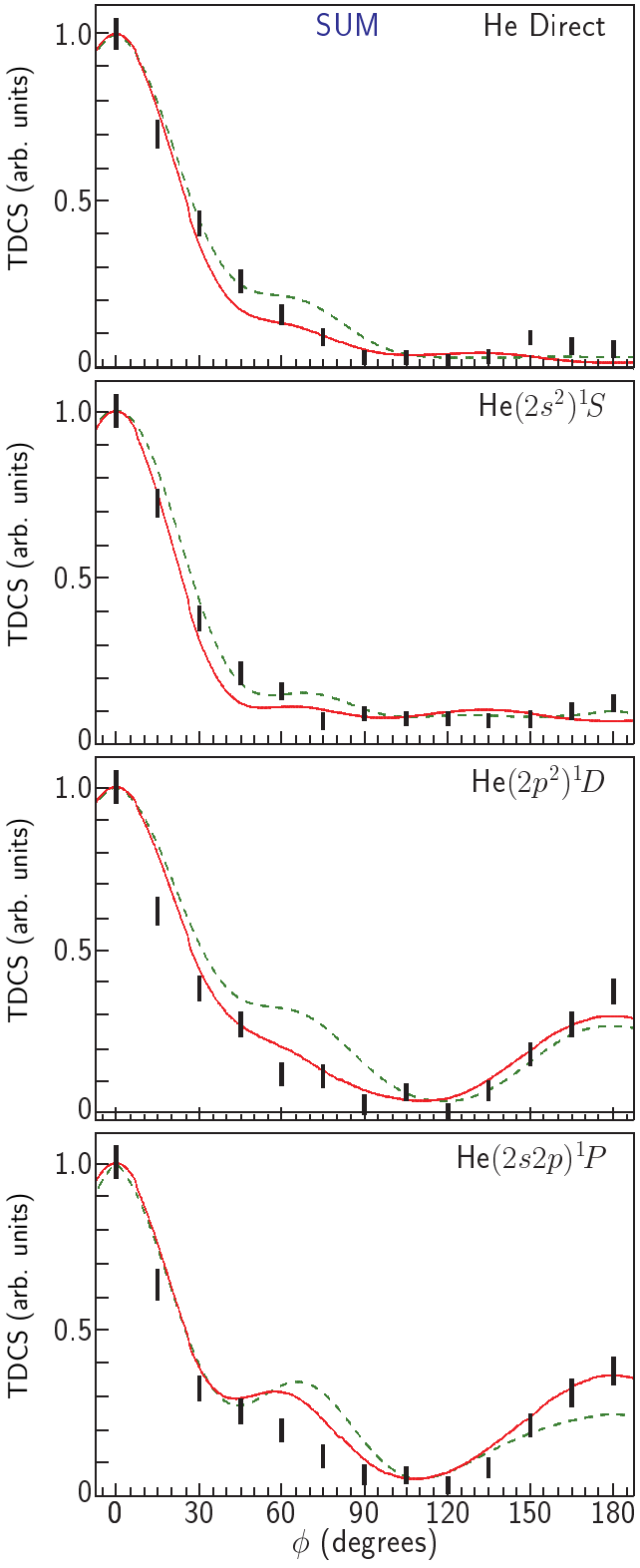

FIG. 6: The weighted sum of the experimental data for 150, 120, and 100 eV incident electron energies (see text), compared with the DWB2-RMPS calculation for 488 eV (solid line), and the BSRMPS calculation for 120 eV (dashed line). Theory and experiment are normalized to unity at $\phi = 0$.